LASER & PHOTONICS REVIEWS
www.lpr-journal.org

Manipulation of Scattering Spectra with Topology of Light and Matter

*Hooman Barati Sedeh, Danilo G. Pires, Nitish Chandra, Jiannan Gao, Dmitrii Tsvetkov, Pavel Terekhov, Ivan Kravchenko, and Natalia Litchinitser**

Structured lights, including beams carrying spin and orbital angular momenta, radially and azimuthally polarized vector beams, as well as spatiotemporal optical vortices, have attracted significant interest due to their unique amplitude, phase front, polarization, and temporal structures, enabling a variety of applications in optical and quantum communications, micromanipulation, and super-resolution imaging. In parallel, structured optical materials, metamaterials, and metasurfaces consisting of engineered unit cells—meta-atoms, opened new avenues for manipulating the flow of light and optical sensing. While several studies explored structured light effects on the individual meta-atoms, their shapes are largely limited to simple spherical geometries. However, the synergy of the structured light and complex-shaped meta-atoms has not been fully explored. In this paper, the role of the helical wavefront of Laguerre–Gaussian beams in the excitation and suppression of higher-order resonant modes inside all-dielectric meta-atoms of various shapes, aspect ratios, and orientations, is demonstrated and the excitation of various multipolar moments that are not accessible via unstructured light illumination is predicted. The presented study elucidates the role of the complex phase distribution of the incident light in shape-dependent resonant scattering, which is of utmost importance in a wide spectrum of applications ranging from remote sensing to spectroscopy.

1. Introduction

A century after the pioneering work of Gustav Mie, exploring various scattering phenomena in micro- and nanoparticles with both single and cluster configuration is still an active field of research and has enabled several promising applications ranging from biological agent detection to the enhancement of nonlinear interactions.[1–3] While early studies were primarily focused on the collective excitation of electromagnetic waves and electrons at metallic interfaces,[4,5] high refractive index engineered dielectric nanoparticles, or meta-atoms, have been shown to provide an alternative route to manipulate light through the excitation of different cavities, or Mie resonances, which depend on both the material and topology of the meta-atoms.[6–16] In particular, these types of resonances become prominent when the meta-atom is either made of a high refractive index material or its size is comparable to the free space wavelength of light.[5] Recently, a variety of high-index materials including germanium,[17–19] gallium nitride,[20–23] silicon,[24–26] and titanium dioxide[27–29] has been used to explore various radiating and non-radiating states within meta-atoms consisting of a single or a cluster of subwavelength particles of different geometries and configurations, such as trimer, quadrumer, and hexamer.[30–32] In addition to the studies of resonant excitations of individual meta-atoms, two-dimensional periodic arrangements of these subwavelength particles, called metasurfaces, have been also shown to facilitate many exotic phenomena and applications, including beam steering,[33–35] actively controlled scattering patterns,[36–38] holography,[39–41] nonlinear harmonic generation,[42–45] Kerker, anti-Kerker, and transverse Kerker effects.[10,46–48] Moreover, an immense effort has also been put into understanding the underlying physical mechanism of Mie resonances for both types of plasmonic and all-dielectric materials, which significantly contributed to this emerging field of research.[49–55] Nevertheless, it is noteworthy that a majority of the related studies in the realm of light–matter interactions with complex resonant meta-atoms were limited to conventional Gaussian light beams. However, in parallel, several approaches including spiral phase plates,[56,57] q-plates,[58–60] spatial light modulators (SLM),[61] and optical metasurfaces[33,62,63] have been developed to generate and manipulate more complex beams, which has led to the emergence of a new category of light beams known as structured light.[64–66]

Structured lights, including beams with a spin and orbital angular momentum (SAM and OAM, respectively), radially and azimuthally polarized vector beams, and spatiotemporal optical

H. Barati Sedeh, D. G. Pires, N. Chandra, J. Gao, D. Tsvetkov, P. Terekhov, N. Litchinitser
Department of Electrical and Computer Engineering
Duke University
Durham, NC 27708, USA
E-mail: natalia.litchinitser@duke.edu
I. Kravchenko
Center for Nanophase Materials Sciences
Oak Ridge National Laboratory
Oak Ridge, TN 37831, USA

The ORCID identification number(s) for the author(s) of this article can be found under https://doi.org/10.1002/lpor.202200472

DOI: 10.1002/lpor.202200472

vortices have been shown to enable a plethora of distinct light–matter interactions and applications in optical communication, particle manipulation, quantum information processing, sensing, and microscopy.[65] In the context of meta-optics, several studies indicated that the properties of light beams themselves can be engineered to excite new resonances in the case of, at least, simple spherical particles. In particular, Wozniak et al. demonstrated that by tailoring the spatial structure of a light beam, individual multipole resonances can be selectively excited while other multipoles are simultaneously suppressed.[67] Moreover, Das et al. theoretically predicted the possibility of manipulating the scattering properties of spherical particles using engineered radially polarized (RP) and azimuthally polarized (AP) light beams,[68] while Zeng et al. discussed the excitation and applications of the magnetic moment within all-dielectric silicon cone using a tightly focused AP light beam.[69] Furthermore, the combination of two RP and AP vector beams for achieving tunable unidirectional scattering has been discussed in.[70,71] In addition, the interference of various Mie-type resonances has been shown to enable unique spectral properties of all-dielectric structures. In this perspective, it was demonstrated that the electric and toroidal dipole moments can destructively interfere with one another, leading to zero scattering with simultaneous confinement of fields within the nanoresonator. Such a non-radiating mode, called an anapole state,[72] has recently gained significant attention owing to its potential applications for cloaking, nonlinear optics, and wireless power transmission.[73–75] In a related study, a particular spatiotemporal beam, the so-called flying doughnut pulse has been utilized to enable an anapole moment within an all-dielectric sphere.[76] The possibility of exciting different kinds of anapole states via two antiphase counter-propagating beams with radial and azimuthal polarization has also been discussed in.[77,78] In a more recent study, Saadabad et al. have theoretically investigated the toroidal dipole and anapole excitation in a dielectric nanodisk by the tightly focused RP beam and the focused doughnut pulse.[79] Finally, structured light-induced Mie resonances have been also exploited in the context of nonlinear optics. For instance, cylindrical vector beams have been utilized to selectively excite the desired multipolar moments such that both second and third harmonics are generated inside AlGaAs and Si scatterers, respectively.[80,81]

Despite significant progress in the field of structured light interaction with resonant Mie particles, the majority of the studies focused on spherically or cylindrically symmetric particles,[82,83] while the synergy of structured light beams and complex shaped meta-atoms has not been fully explored. Here, we show that the interaction of an OAM-carrying light beam, in particular Laguerre–Gaussian (LG) beam, with nanocuboids and randomly tilted meta-atoms with varying aspect ratios results in entirely new scattering characteristics and degrees of freedom for selective excitation, suppression, and manipulation of individual resonant modes of these scatterers as compared to those obtained with a conventional Gaussian beam and spherically/cylindrically symmetric particles, opening new prospects for applications such as remote sensing and communications in scattering media.

2. Theoretical Formulation

We start with a multipole decomposition of the fields scattered by the particle to investigate the role of the beam structure, such as an intensity modulation and a helical wavefront of the incoming light beam, on the optical response of a stand-alone arbitrary shape meta-atom.[84,85] Here, the surrounding environment is assumed to be free space, while the incident wave is considered to be linearly polarized along the y axis, i.e., $(0, \hat{e}_y, 0)$, with its wave vector pointing toward $\boldsymbol{k} = (k_x, 0, 0)$ direction as it is schematically shown in **Figure 1**. Upon the interaction of light with the meta-atom, the induced polarization is related to the field distributions within the particle via $\boldsymbol{P} = \epsilon_0(\epsilon_p - \epsilon_d)\boldsymbol{E}_p$, where ϵ_0, ϵ_p, and ϵ_d are the free space, particle, and surrounding medium dielectric constants, respectively, and $\boldsymbol{E}_p$ is the total electric field inside the scatterer. The scattered field is given by the superposition of different multipole moments (up to the electric octupole term) as[85]

$$\boldsymbol{E}_{sct}(\boldsymbol{n}) = \frac{k_0^2 \exp(ik_0 r)}{4\pi\epsilon_0 r}\left([\boldsymbol{n}\times[\boldsymbol{D}\times\boldsymbol{n}]] + \frac{1}{c}[\boldsymbol{m}\times\boldsymbol{n}] + \frac{ik_0}{6}\left[\boldsymbol{n}\times\left[\boldsymbol{n}\times\hat{Q}\boldsymbol{n}\right]\right] + \frac{ik_0}{2c}\left[\boldsymbol{n}\times\hat{M}\boldsymbol{n}\right] + \frac{k_0^2}{6}\left[\boldsymbol{n}\times\left[\boldsymbol{n}\times\hat{O}(\boldsymbol{n}\boldsymbol{n})\right]\right]\right) \quad (1)$$

where $\boldsymbol{D}$ corresponds to the exact total electric dipole (TED) consisting of both electric dipole (ED) and toroidal dipole (TD) moments, $\boldsymbol{m}$ is the exact magnetic dipole (MD) moment, and $\hat{Q}$, $\hat{O}$, and $\hat{M}$ represent the electric quadrupole (EQ), electric octupole (EO), and magnetic quadrupole tensors, respectively; $\boldsymbol{n} = \boldsymbol{r}/r$ is the unit vector directed from the particle's center toward an observation point, and c is the speed of light in vacuum. Using these notations, the far-field scattered power can be readily related to the scattered fields of Equation (1) with the aid of a time-averaged Poynting vector as $dP_{Sct} = 0.5\sqrt{\epsilon_0/\mu_0}|E_{Sct}|^2 r^2 d\Omega$, wherein $d\Omega = \sin\theta d\theta d\varphi$ represents the solid angle.[84–86] Therefore, combining Equation (1) with the given relation of scattered power and performing the integration over the total solid angle, the scattering cross-section, defined as $\sigma_{Sct} = P_{Sct}/I_0$, with I_0 being the maximum beam intensity in a focal plane, can be written as follows [85]

$$\sigma_{Sct} \approx \frac{k_0^4}{12\pi\epsilon_0^2\eta_0 I_0}|\boldsymbol{D}|^2 + \frac{k_0^4\mu_0}{12\pi\epsilon_0\eta_0 I_0}|\boldsymbol{m}|^2 + \frac{k_0^6}{1440\pi\epsilon_0^2\eta_0 I_0}\sum_{x_1,x_2}\left|Q_{x_1x_2}\right|^2 + \frac{k_0^6\mu_0}{160\pi\epsilon_0\eta_0 I_0}\sum_{x_1,x_2}\left|M_{x_1x_2}\right|^2 + \frac{k_0^8}{3780\pi\epsilon_0^2\eta_0 I_0}\sum_{x_1,x_2,x_3}\left|O_{x_1x_2x_3}\right|^2 \quad (2)$$

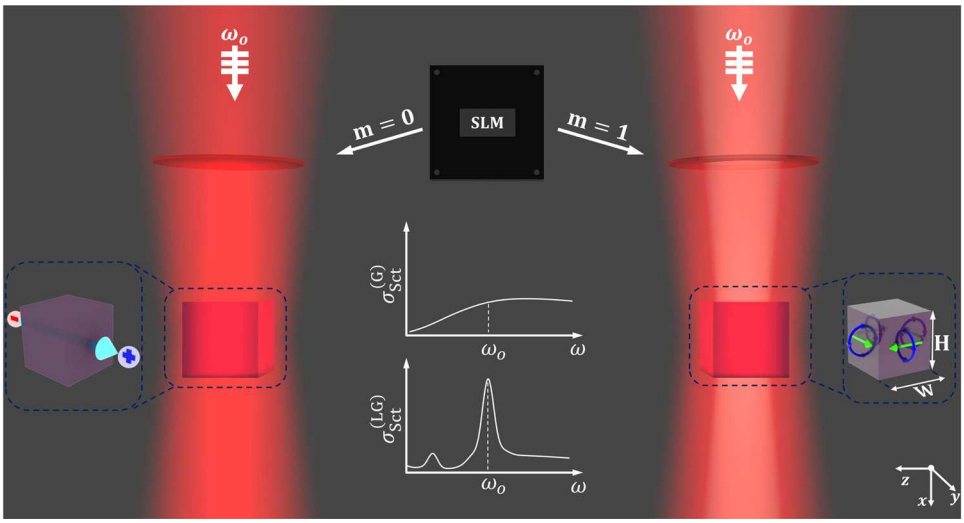

Figure 1. The schematic depiction of Mie resonance manipulation using OAM beams. By utilizing an SLM to change the structural features of the incoming ***y***-polarized light beam, from a Gaussian beam having a topological charge of $m = 0$ to LG possessing $m = 1$, the excited multipole moments within the polycrystalline silicon particle can be manipulated and "turned-on and off" on demand.

where η_0 and μ_0 are the impedance and permeability of free space, respectively, and x_1, x_2, and x_3 represent the different components of each tensor. As was shown in ref. [85], each of the presented moments in Equation (2) can be expressed in terms of the induced current within the particle ($\boldsymbol{J} = \partial \boldsymbol{P}/\partial t$) as

$$
\begin{aligned}
\boldsymbol{D} &= \frac{i}{\omega}\int j_0\left(k_0 r'\right)\boldsymbol{J}\left(\boldsymbol{r}'\right)d\boldsymbol{r}' + \frac{ik_{\mathrm{d}}^2}{2\omega}\int \frac{j_2\left(k_{\mathrm{d}}r'\right)}{\left(k_{\mathrm{d}}r'\right)^2}\left[3\left(\boldsymbol{r}'\cdot\boldsymbol{J}\right)\boldsymbol{r}' - r'^2\boldsymbol{J}\right]d\boldsymbol{r}' \\
\boldsymbol{m} &= \frac{3}{2}\int \frac{j_1\left(k_{\mathrm{d}}r'\right)}{k_{\mathrm{d}}r'}\left[\boldsymbol{r}'\times\boldsymbol{J}\right]d\boldsymbol{r}' \\
\hat{M} &= 5\int \frac{j_2\left(k_{\mathrm{d}}r'\right)}{\left(k_{\mathrm{d}}r'\right)^2}\left(\left[\boldsymbol{r}'\times\boldsymbol{J}\right]\otimes\boldsymbol{r}' + \boldsymbol{r}'\otimes\left[\boldsymbol{r}'\times\boldsymbol{J}\right]\right)d\boldsymbol{r}' \\
\hat{Q} &= \frac{3i}{\omega}\int \frac{j_1\left(k_{\mathrm{d}}r'\right)}{k_{\mathrm{d}}r'}\left[3\left(\boldsymbol{r}'\otimes\boldsymbol{J}+\boldsymbol{J}\otimes\boldsymbol{r}'\right) - 2\left(r'\cdot\boldsymbol{J}\right)\bar{\bar{I}}\right]d\boldsymbol{r}' + \frac{i6k_{\mathrm{d}}^2}{\omega}\int \frac{j_3\left(k_{\mathrm{d}}r'\right)}{\left(k_{\mathrm{d}}r'\right)^3}\left[5\left(\boldsymbol{r}'\cdot\boldsymbol{J}\right)\boldsymbol{r}'\otimes\boldsymbol{r}' - r'^2\left(\boldsymbol{J}\otimes\boldsymbol{r}'+\boldsymbol{r}'\otimes\boldsymbol{J}\right) - \left(\boldsymbol{J}\cdot\boldsymbol{r}'\right)r'^2\bar{\bar{I}}\right]d\boldsymbol{r}' \\
\hat{O} &= \frac{15i}{\omega}\int \frac{j_2\left(k_{\mathrm{d}}r'\right)}{\left(k_{\mathrm{d}}r'\right)^2}\left(\boldsymbol{J}\otimes\boldsymbol{r}'\otimes\boldsymbol{r}' + \boldsymbol{r}'\otimes\boldsymbol{J}\otimes\boldsymbol{r}' + \boldsymbol{r}'\otimes\boldsymbol{r}'\otimes\boldsymbol{J} - \hat{A}\right)d\boldsymbol{r}'
\end{aligned}
\tag{3}
$$

where $j_l(x)$ is the lth order spherical Bessel function, k_{d} is the wave number in the surrounding medium, $\bar{\bar{I}}$ is the 3×3 unit tensor, and the operators of $\cdot$, $\times$, and $\otimes$ represent the scalar, vector, and tensor products, respectively. It should be noted that $\hat{A}$ is an auxiliary tensor whose components are obtained according to $A_{x_1x_2\,x_3} = \delta_{x_1x_2}V_{x_3} + \delta_{x_1x_3}V_{x_2} + \delta_{x_2x_3}V_{x_1}$, which $x_1 = (x, y, z)$, $x_2 = (x, y, z)$, $x_3 = (x, y, z)$ and δ is the Kronecker delta while $V = 0.2[2(\boldsymbol{r}'\cdot\boldsymbol{J})\otimes\boldsymbol{r}' + r'^2\boldsymbol{J}]$.[85] The expressions given by Equation (3) are known as spherical (exact) multipole moments and are valid for any arbitrary shaped particles regardless of their size and topology. The readers are referred to Section S1 (Supporting Information) for more information about spherical and Cartesian (also known as a long-wavelength approximation) multipole moments. It should be noted that in particular, there are two approaches for studying the light–matter interactions in dielectric meta-atoms. The first method relies on the expansion of electromagnetic fields in terms of the spherical harmonic coefficients, which then can be used to obtain information about the contributing moments for a particular meta-atom.[72,87] The second approach, which has been implemented in this paper, is based on the multipole decomposition of the Cartesian components of the current density inside the particle such that when it is illuminated by an arbitrary shaped beam, the expressions of Equation (3) can be used to describe the optical response of the scatterer.[88,89]

3. OAM-Induced Mie Resonances

To investigate the synergy between the complex-shaped beams and topologies of the meta-atoms, the numerical simulations are carried out using the finite-element method (FEM) implemented in the commercial software COMSOL Multiphysics. In particular, we utilize the Wave Optics Module to solve Maxwell's equations in the frequency domain together with proper boundary conditions. Here, we use a spherical domain filled with air and a radius of 4λ as the background medium, while perfectly matched layers of thickness 0.6λ are positioned outside of the background medium to act as absorbers and avoid undesired scattering. Tetrahedral mesh is also chosen to ensure the accuracy of the results and allow numerical convergence. The refractive index of the polycrystalline silicon, which was obtained from our ellipsometry measurements, is used in our numerical simulation instead of the original COMSOL model for silicon (see Section S2, Supporting Information for more details and comparison) and the standard expression of the LG beam, which is not tightly focused, is directly utilized as the background field with its radial index set to zero[66] as

$$E_{\text{inc}} = C_{\text{m}} \frac{w_0}{w(x)} \left(\frac{\rho\sqrt{2}}{w(x)} \right)^{|m|} \exp\left(-\left(\frac{\rho}{w(x)} \right)^2 - \frac{ik\rho^2}{2R(x)} \right) \exp(-im\varphi)\ \exp(i(1+|m|)\Phi(x)) \tag{4}$$

where in $C_{\text{m}} = E_0\sqrt{1/\pi(|m|!)}$ is the normalization constant, $w(x) = w_0\sqrt{1+(x/x_{\text{R}})^2}$ is the beam size, $R(x) = x[1+(x/x_{\text{R}})^2]$ is the radius of curvature with $w_0 = \lambda$ being the beam waist and x_{R} representing the Rayleigh range. Moreover, the constant m in Equation (4) is known as topological charge (TC) and $\Phi(x) = (\tan(x/x_{\text{R}}))^2$ represents the Gouy phase.[66] As can be seen from Equation (4), the structure of the LG beam differs from the regular Gaussian beam (plane wave) with an extra phase term of $\exp(-im\varphi)$, which leads to a phase singularity along the beam axis ($\hat{e}_{\text{x}}$ direction) and a dark central spot in its cross-section. In this study, we consider two types of particles: polycrystalline silicon cuboids and cylinders with the dimensions of $W \times W \times H$ and $R \times H$, respectively, where W is the width of the sides of the cuboid in y and z directions, R is the radius of the cylinder, and H is the height of the cuboid or cylinder, as shown in Figure 1. Note that the key point in the evaluation of scattering cross-section is the calculation of the induced polarization (or equivalently the currents) within the resonator and then associating the multipolar moments according to the given expression of Equation (3), which do not depend on the illumination type. That is, regardless of the shape of the illuminating beam, once the current distributions within the meta-atoms are obtained via full-wave numerical calculations, the provided expressions of Equation (3) can be readily implemented to determine the optical response of the scatterer.[76,79,90,91]

To investigate the effect of the aspect ratio of the cuboid meta-atom on its scattering characteristics, we fix its height to $H =$ 260 nm and change its width-to-height aspect ratio ($\alpha = W/H$) from 0.5 to 2, while the operating wavelength is swept in the range of 700–1000 nm. The contributions of the various multipolar moments were obtained by integrating the displacement current induced within the meta-atom using Equation (3). The final scattering cross-sections, as well as their normalization, were numerically calculated and are shown in **Figure 2**a,b for the cases of Gaussian (with the topological charge (TC) of $m = 0$) and LG ($m = 1$) illumination, respectively.

By comparing the total scattering cross-sections, we conclude that once the topological charge of the incident beam is changed from $m = 0$ to $m = 1$, the scattering response of the cuboid meta-atom varies significantly, yielding the emergence and suppression of new resonant modes for various aspect ratios. In particular, for $\alpha < 1.5$ the optical response of the nanocuboid is suppressed as the incoming beam is changed from Gaussian (unstructured) to LG (structured) possessing singularity in its phase distribution and a dark central spot in its intensity. However, for $\alpha > 1.5$, new resonant modes emerge at longer wavelengths as the cuboid aspect ratio further increases. Such phenomena are attributed to the coupling of light to various higher-order multipolar moments once its wavefront acquires a helical shape. To further clarify the origins of these newly emerged and suppressed resonant features, we plotted the contribution of each higher-order multipolar moment in Figure 2c,d for the cases of Gaussian and LG illumination. Figure 2c shows that under the Gaussian excitation, the scattering response of the meta-atom is mainly dominated by the lower electric and magnetic dipolar moments while the contributions of quadrupole and octupole moments are almost negligible. On the contrary, in the case of the LG beam, the optical response of the meta-atom is governed by the higher quadrupolar and octupolar moments, while the dipolar counterparts become suppressed. In particular, when the aspect ratio varies between $1.5 < \alpha < 2$, new resonant features emerge within the cuboid meta-atom whose spectral positions depend on the meta-atom dimensions and are not accessible via Gaussian excitation. Taking $\alpha = 2$ as a particular example, it is evident that the response of the meta-atom under LG illumination is dominated by the EQ, MQ, and EO moments, at $\lambda = 945$, $\lambda = 870$, and $\lambda = 725$ nm, respectively.

As was mentioned earlier, the synergy of structured light beam and complex-shaped meta-atoms has not been fully explored, and therefore, it would be of interest to study the light–matter interaction between OAM-carrying light beams and different shape meta-atoms. In this perspective, we have also investigated the effect of nonzero azimuthal LG mode on the optical response of a polycrystalline silicon-based nanocylinder. As before, we fixed the height of the cylinder to $H = 260$ nm, while its aspect ratio, $\beta = R/H$, changes from 0.5 to 2 over the wavelength range of 700–1000 nm. Following the same procedure, the multipole

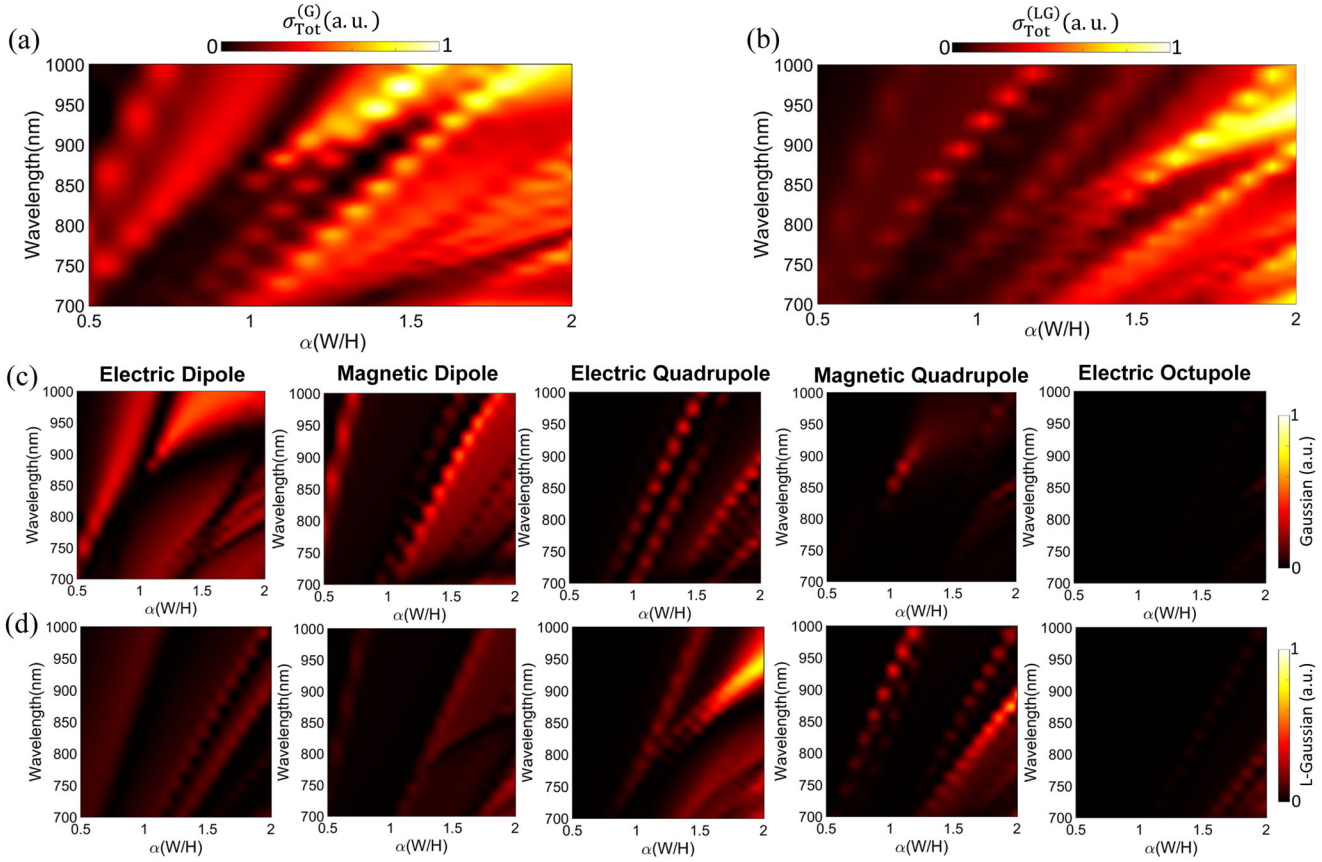

Figure 2. The normalized total scattering cross-section of the cuboid meta-atom under the illumination with a) Gaussian ($m = 0$) and b) LG ($m = 1$) beams. The contribution of ED, MD, EQ, MQ, and EO multipolar moments excited within the meta-atom as functions of aspect ratio and operating wavelength under the illumination of c) Gaussian and d) Laguerre–Gaussian beams.

decompositions of such a meta-atom are calculated and collated in **Figure 3**.

Figure 3a,b shows that the presence of the phase gradient (due to the helical wavefront of the incoming beam) changes the overall scattering response of the polycrystalline silicon-based cylindrical meta-atom by adding and suppressing various resonant modes. In particular, by comparing the results in panels (a) and (b), it is clear that for the aspect ratio in the range of $1 < \beta < 1.5$, the scattering response of the meta-atom is suppressed, while for $\beta > 1.5$, new resonant peak emerged. The contribution of each multipolar moment is also obtained based on Equation (3) at each operating wavelength and its results for both types of illumination are shown in Figure 3c,d. As can be seen, for Gaussian incidence, the scattering response of the cylindrical meta-atom is mainly dominated by the ED and MD contributions, while once the topological charge of the incoming wave changes to $m = 1$, higher order multipolar moments enhance significantly. The readers are referred to Section S3 (Supporting Information) for more information about the effect of geometrical tuning on the optical response of the meta-atoms.

According to the obtained results in Figures 2 and 3, it is evident that while the geometrical tuning of the meta-atoms yields the excitation of different moments, the unique structure of the incident LG beam can also lead to the emergence of new resonant features such as electric and magnetic quadrupole moments. These results can be understood by considering the interplay between the gradient of the incident electric field and its phase distribution. In particular, once the topological charge of the excitation source changes from $m = 0$ to $m = 1$, the sign of the gradient of the electric field, $\nabla_{\perp}\boldsymbol{E}$, varies across the phase change of the beam, yielding the excitation of different components of the quadrupole tensor. In other words, various components of the quadrupolar tensors (regardless of their kinds) can be addressed by manipulating the phase of the incident wave (changing the topological charge), which in turn makes the OAM charge tuning an alternative approach for enabling the new degrees of freedom in the manipulation of the scattering response. We note that although such a behavior has been observed previously in the realm of atomic and particle physics, to the best of our knowledge, it has not yet been considered in the context of Mie scattering for arbitrary shape meta-atoms. To further elaborate on the concept of OAM-beam-based manipulation of the scattering response, we fix the aspect ratios of the cuboid and cylindrical meta-atoms to $\alpha = 1$, and $\beta = 0.65$, respectively, and investigate their scattering responses for different azimuthal LG modes with the values of $m = [0, 1, 2, 3]$ as shown in **Figure 4**.

Panels (a) and (b) show that the helical wavefront of the incoming wave can dramatically alter the optical response of the subwavelength meta-atoms by adding/suppressing extra resonant peaks in their scattering spectra. In particular, the

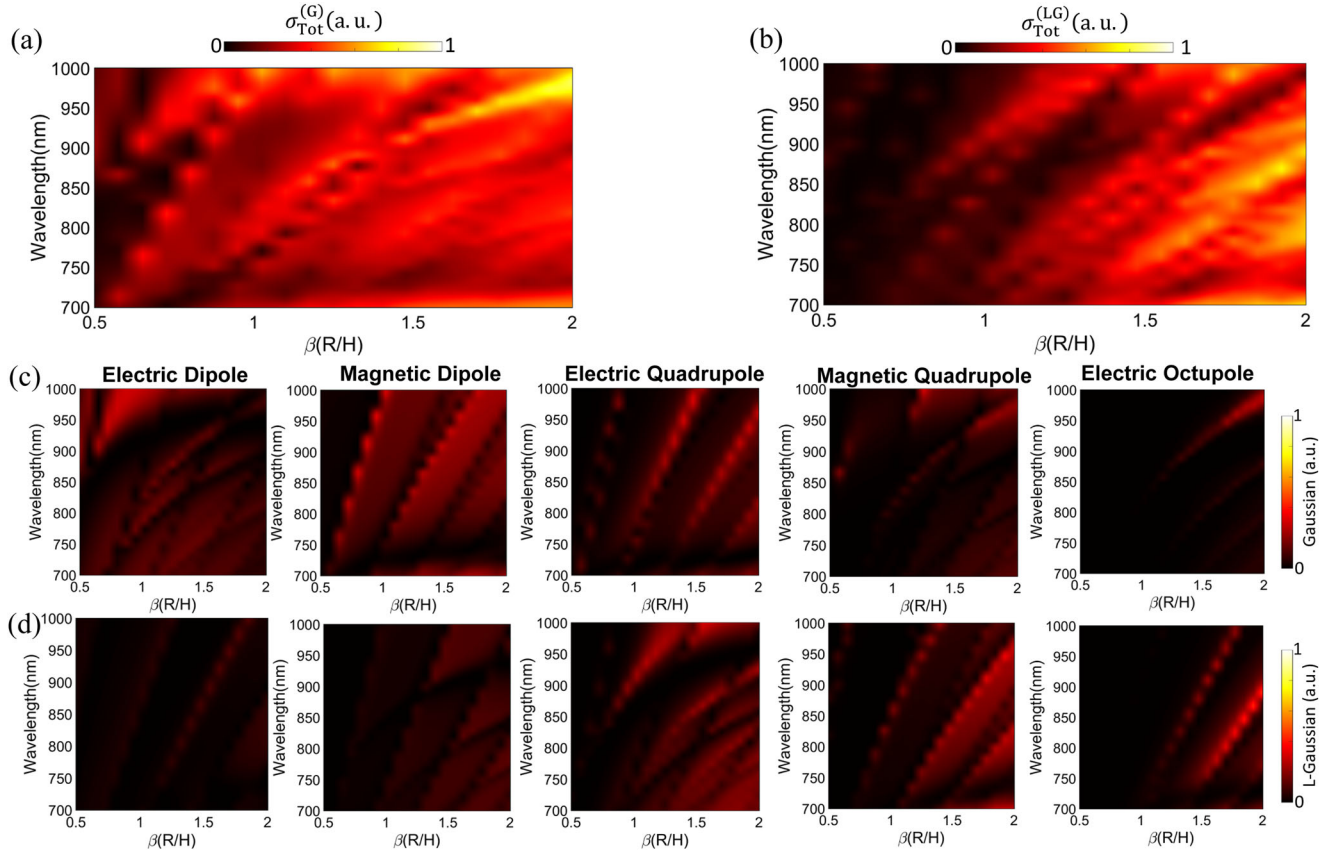

Figure 3. The normalized total scattering cross-section of the cylindrical meta-atom under the illumination of an LG beam with topological charges of a) $m = 0$ and b) $m = 1$. The contribution of spherical multipolar moments excited within the meta-atom as functions of aspect ratio and operating wavelength under the illumination of c) Gaussian and d) Laguerre–Gaussian beams.

topological charge of the incoming light beam leads to the excitation/suppression of new resonant modes, which are not accessible under Gaussian or plane wave illumination. To investigate the origin of these peaks, the spherical multipole decomposition for the cases of $m = 0$ and $m = 1$ was performed for both types of meta-atoms as shown in Figure 4c–f. In particular, panel (c) of Figure 4 demonstrates that the scattering response of the cubic meta-atom under Gaussian illumination is mainly dominated by the electric field contribution, with a single peak of magnetic quadrupole at $\lambda = 843$ nm. However, once the topological charge of the incident wave changes to $m = 1$, the electric contribution of the optical response of the cubic meta-atom is suppressed significantly, while a new MQ resonant mode emerges at the spectral wavelength of $\lambda = 915$ nm. The newly emerged MQ peak (point P_4) demonstrates a strong tendency to shift toward longer wavelengths, making itself spectrally decoupled from the initial peak (P_1/P_3), while the electric counterpart is weakly shifted toward the shorter wavelengths. Such an OAM-induced behavior leads the scattering response of the meta-atom to be mainly dominated by the MQ contribution at the operating wavelength of 915 nm, whereas it was previously influenced by the electric dipole moment (P_2). Similar behavior is also evident for the cylindrical meta-atom as it is shown in Figure 4e,f. In particular, at the specific point of P_5 ($\lambda = 975$ nm), at which the far-field scattering spectrum of the meta-atom has a dip with a simultaneous zero ED moment, the OAM of the incoming light field alters the scattering response in such a way that the anapole state is changed to MQ resonant mode (see Section S4, Supporting Information for more details on the effect of beam waist and structure of the incident lights).

Figure 5 shows the distribution of the electric intensity within the cubic and cylindrical meta-atoms at the corresponding wavelengths of points $P_1 - P_6$. Upon Gaussian illumination, merely the M_{xz} (also M_{zx}) component of the magnetic quadrupole tensor is excited, which in turn leads the field distribution inside the cubic meta-atom at point P_1 to exhibit four hot spots with magnetic field rotating around them as shown with red arrows in Figure 5a. At point P_2, which corresponds to the excitation of ED moment, the electric field is confined at the center of the meta-atom, while the magnetic fields are rotating around it as it is demonstrated in Figure 5b. However, once the topological charge of the incoming beam is changed to $m = 1$, both the diagonal (M_{xx} and M_{zz} for P_4) and off-diagonal (M_{yz} and M_{zy} for P_3) components of magnetic quadrupole tensor are excited leading to the similar field distribution as that of P_1 (Figure 5c,d). Note that the field distribution at point P_3 is the same as that of point P_1 but with a $\pi/2$ rotation which corresponds to the transformation of $M_{xz} \rightarrow M_{yz}$. On the other hand, the intensity distribution the of cylindrical meta-atom at point P_5 corresponds to the excitation of anapole dark mode, which manifests itself as

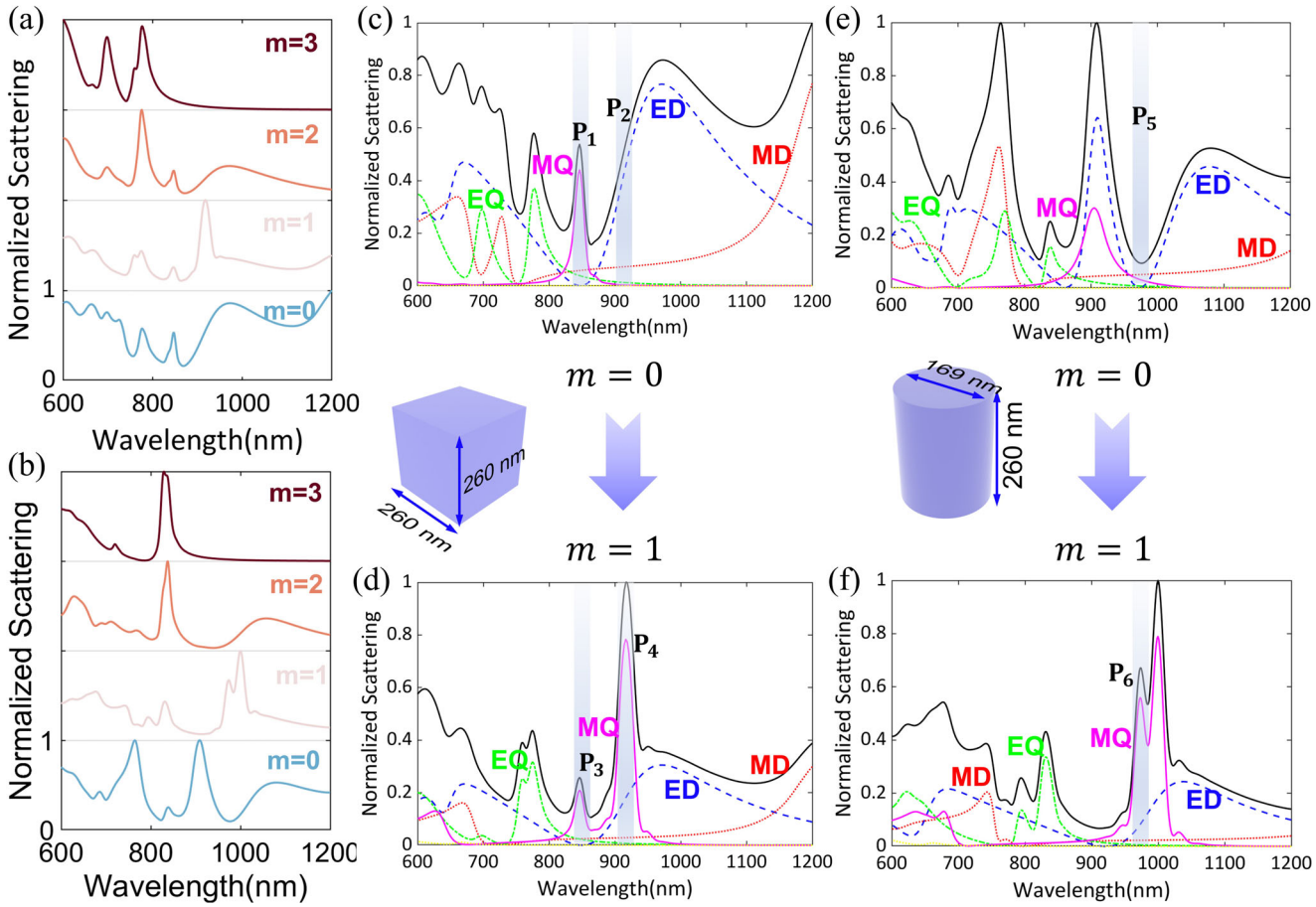

Figure 4. The total scattering cross-section of a) cubic, and b) cylindrical meta-atoms for four different values of the topological charge $m = [0, 1, 2, 3]$ as functions of wavelength when their corresponding aspect ratios are fixed to $\alpha = 1$ and $\beta = 0.65$, respectively. The baseline for each of the spectra has an offset of 1 au. The spherical multipole decomposition of the c,d) cube and e,f) cylinder meta-atom under unstructured ($m = 0$) (c,e) and structured ($m = 1$) (d,f) light illuminations. Upon a change in the wavefront of the incoming light beam, newly resonant peaks are emerged/suppressed.

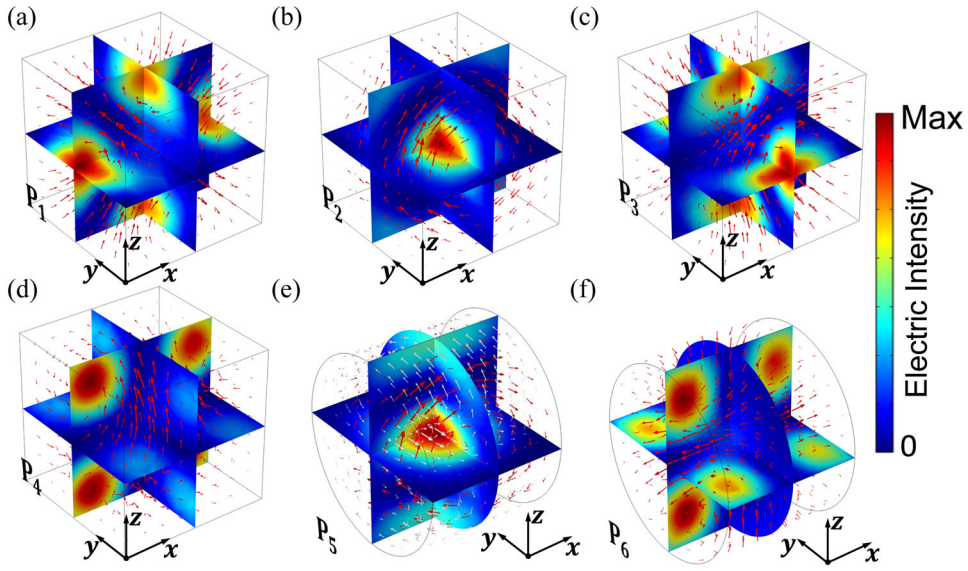

Figure 5. The intensity distributions within the cubic and cylindrical meta-atoms at six particular points of $P_1 - P_6$ corresponding to a) shape-induced MQ, b) shape-induced ED, c) shape-induced MQ with $\pi/2$ rotation, d) OAM-induced MQ, e) shape-induced anapole, and f) OAM-induced MQ moment. The red arrows demonstrate the magnetic field direction, while their white counterpart represents the electric field.

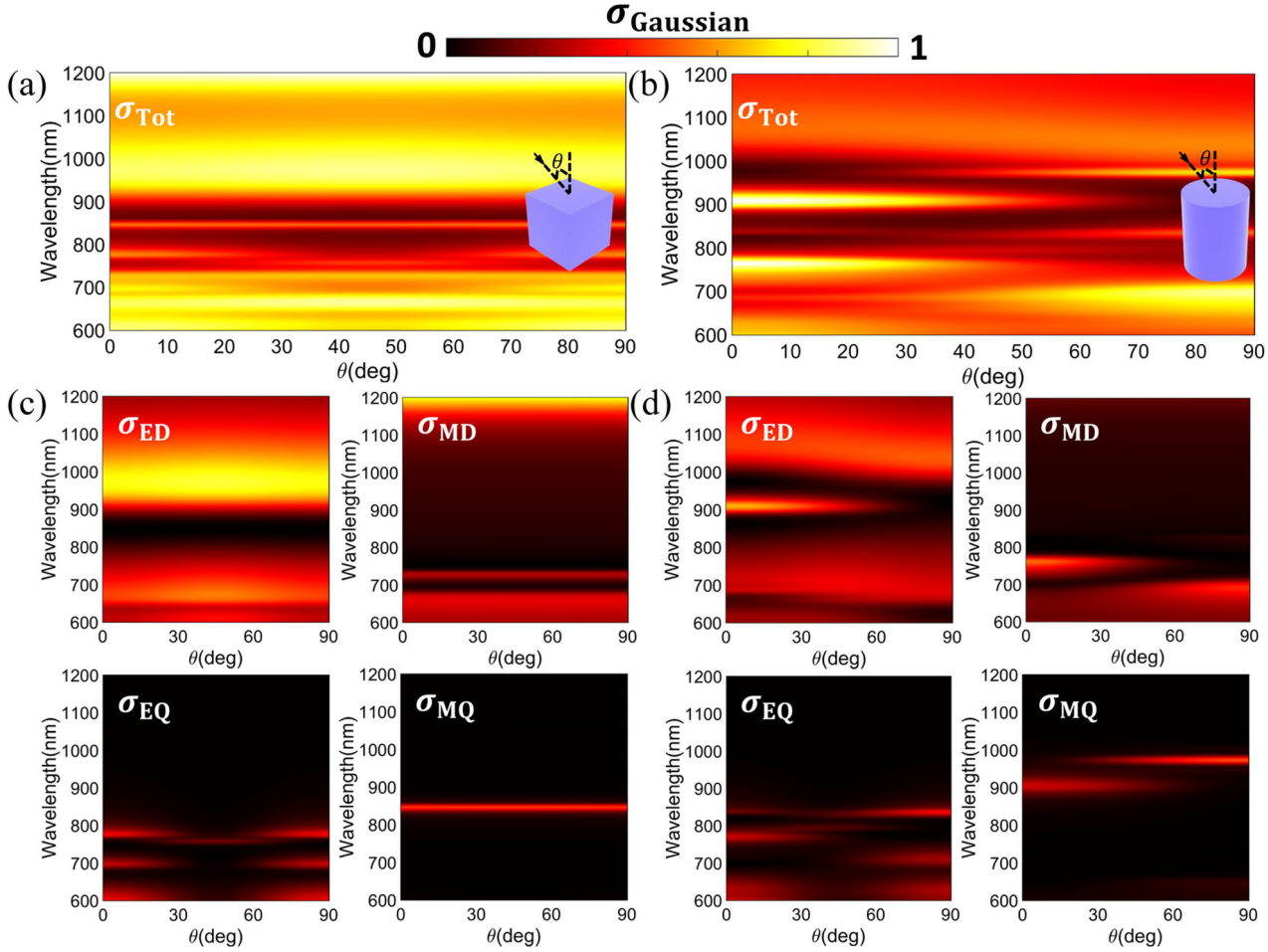

Figure 6. The normalized total scattering cross-section of a) cubic and b) cylindrical meta-atoms under Gaussian light incidence with different angles ranging from $0° < \theta < 90°$ as functions of the operating wavelength. For both meta-atoms, the incident light beam is Gaussian with $m = 0$. c,d) The calculated spherical (exact) multipolar moments up to MQ order for both meta-atoms with their aspect ratios being $\alpha = 1$ and $\beta = 0.65$, respectively. As opposed to the optical response of the cubic meta-atom, which is symmetric with respect to the angle of incidence, the response of the cylindrical meta-atom is asymmetric.

the circulating magnetic field (red arrows) and poloidal electric field distribution (white arrows). However, upon the variation of the incoming light wavefront, such a dark mode is changed to bright MQ mode with an alternation near-field field distribution as shown in Figure 5f. Therefore, we conclude that different scattering behaviors arise due to the formation of distinct current distributions within the resonator, which lead to the excitation of different components of contributing moments such as MQ tensor. These results clearly show that the helical wavefront of the incident light beam can significantly affect the scattered radiation pattern of both meta-atoms, potentially enabling the possibility of spectral tuning of the scattering pattern that can be used in all-dielectric optical nanoantennas.[92]

4. Angular Dependency of OAM-Induced Resonances

In the previous section, we investigated the optical response of the meta-atoms under the normal angle of incidence for Gaussian and LG illuminations. However, as it was shown in ref. [93], under plane wave illumination, the angle of incidence can also alter the coupling efficiency of a particular Mie resonant mode within an array of silicon disk meta-atoms. Nevertheless, to the best of our knowledge, structured light–matter interactions with all-dielectric subwavelength meta-atoms at oblique incidence have not been investigated in detail. Therefore, this section is devoted to the study of angular dependency of the presented meta-atoms with OAM-carrying light beams. For this purpose, we fixed the aspect ratio of cubic and cylindrical meta-atoms to $\alpha = 1$ and $\beta = 0.65$, respectively, and sweep the angle of incidence from $0° < \theta < 90°$ over the wavelength range of 600 nm $< \lambda <$ 1200 nm. As the starting point, we assume the unstructured light illumination (i.e., $m = 0$), such that merely the effect of angular dependency of the meta-atoms is revealed. **Figure 6**a shows that due to the symmetrical topology of the cubic meta-atom, its scattering response is also symmetric with respect to the angle of incidence, whereas for the case of cylindrical meta-atom, the scattering response changes to asymmetric as

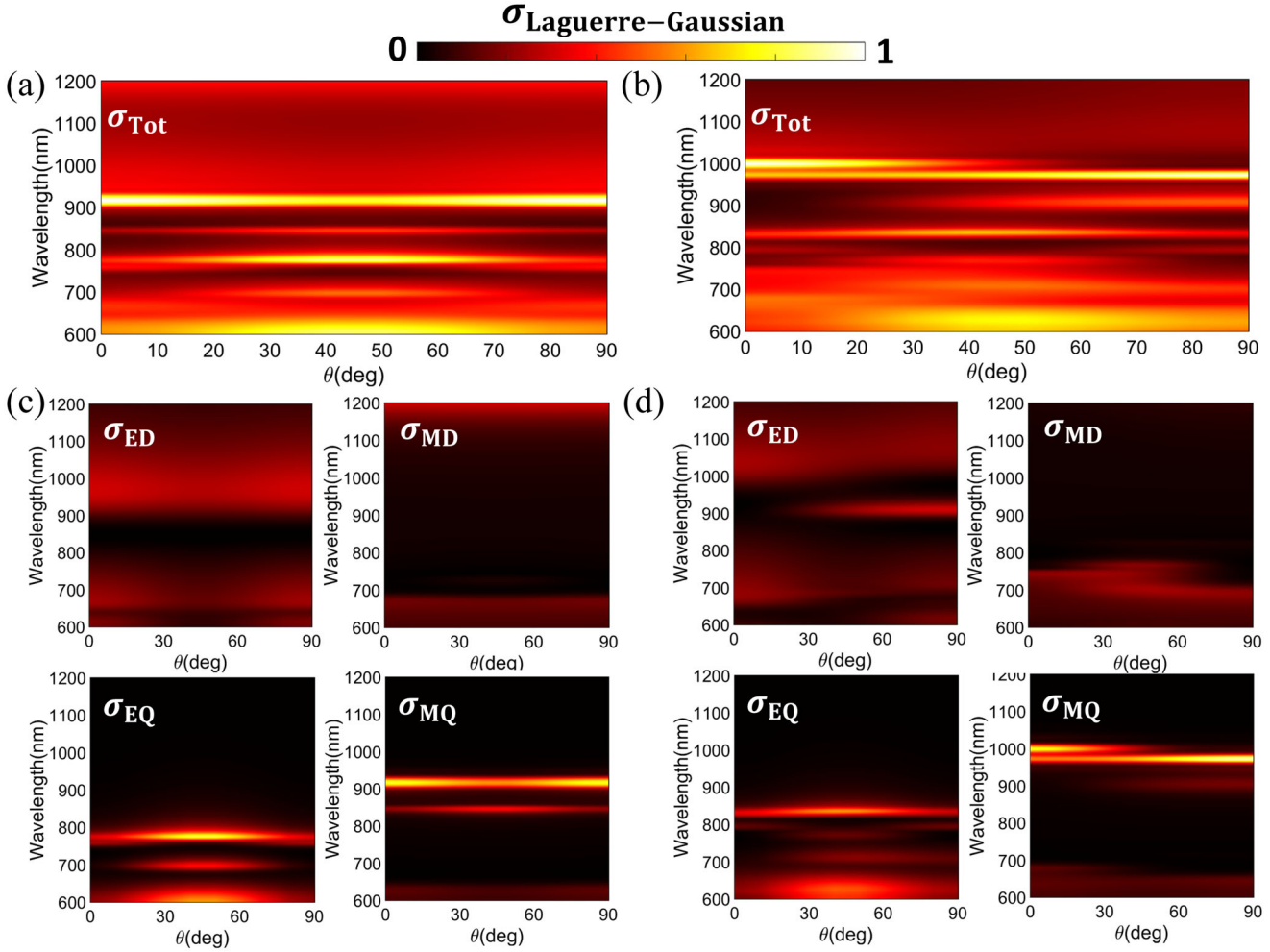

Figure 7. The normalized total scattering cross-section of a) cubic and b) cylindrical meta-atoms under the LG illumination as functions of incident angle. c,d) The calculated spherical (exact) multipolar moments up to MQ order for both meta-atoms with their aspect ratios being $\alpha = 1$ and $\beta = 0.65$, respectively.

the radius to the height (aspect) ratio of this meta-atom, β, is not unity. In particular, the multipole decomposition results shown in Figure 6c,d demonstrates that the angle of incidence yields the excitation/suppression of new resonant modes for both types of meta-atoms, revealing another mechanism for engineering the Mie-type resonances within the meta-atoms. Such behavior is attributed to the change of different components of multipolar moments once the direction of illumination is changed. For instance, under frontal illumination (i.e., $\theta = 0°$), the off-diagonal Q_{xy}/Q_{yx} and M_{xz}/M_{zx} components of the electric and magnetic quadrupole tensors are excited, respectively, which eventually lead to comparable peaks of these moments in the scattering spectra, as shown in Figure 6c. However, once the angle of incidence changes to $30° < \theta < 60°$, the contribution of Q_{xy}/Q_{yx} is suppressed significantly while M_{xz}/M_{zx} remains the same, leaving the scattering response to be dominated by MQ moments over the wavelength range of 600 nm $< \lambda <$ 1200 nm. Such an angular dependency behavior is not limited to a particular shape and the same trend is also evident for the cylindrical meta-atom, as it is shown in Figure 6d. Taking the EQ and MQ moments as the example, we note that for the frontal and lateral ($\theta = 90°$) illumination, both M_{xz}/M_{zx} and Q_{xy}/Q_{yx} components of the MQ and EQ tensors are excited within the meta-atom with different amplitudes. While Figure 6, demonstrates the direction of illumination as another method of engineering Mie-type resonances, the combination of incident angles and the structure of the incoming light has not yet been thoroughly studied. To fill this gap, in this section we investigate the effect of such a combination on the optical response of the presented meta-atoms.

Figure 7a,b shows that the phase-asymmetry of the incident light beam results in significant changes in the optical response of both meta-atoms at different angles of incidence. In particular, the magnitude of phase asymmetry-induced resonances can also be manipulated by the illumination angle (or by the change of the meta-atom orientation), besides the OAM tuning approach. Therefore, contrary to the Gaussian case, in the case of LG illumination shown in Figure 7c, the EQ moment is dominated by the incident angles of $30° < \theta < 60°$, which is attributed to the excitation of both diagonal (Q_{xx}, Q_{yy}, and Q_{zz}) and off-diagonal (Q_{yz}/Q_{zy}) components rather than merely off-diagonal terms

(Figure 6c). In addition to the EQ moment, both the contributions of the diagonal and off-diagonal components of the MQ tensor are boosted, leading to two different branches of resonant peaks, that we call conventional (related to M_{yz}/M_{zy} excitation) and topological charge-induced (related to the emergence of M_{xx} and M_{zz}), at different directions of illumination as shown in Figure 7c. We note that the same behavior for the cylindrical meta-atom can be seen in Figure 7d, whereas the optical response of the meta-atom exhibits asymmetric behavior. In particular, the features of the MQ resonant scattering are different for frontal and lateral LG illumination, which is attributed to the suppression of M_{yy} components under lateral illumination ($\theta = 90°$), while the behavior of the EQ moment is purely symmetrical since the excited components of Q_{xx}, Q_{yy}, Q_{zz}, and Q_{yz} (Q_{zy}) remain unchanged for both angles of incidences.

These results demonstrate the role of the phase gradient and the illumination direction in the excitation of Mie resonances in the arbitrary shaped all-dielectric meta-atoms. Although the interactions of structured light with non-spherical meta-atoms such as a cluster of spheres,[94] split ring resonator,[95] rods,[96] and prisms[97] have been studied previously with AP/RP and Hermite Gaussian beams, the role of the phase gradient of the Laguerre–Gaussian beams in the excitation and suppression of higher-order resonant modes inside all-dielectric meta-atoms of various shapes, aspect ratios, and orientations has not been explored to date. Complementary to recent experimental studies that addressed some aspects of the OAM beam interaction with spherical[98] and chiral nanostructures,[99] our study predicted the possibility of the excitation of various multipolar moments which are not accessible via unstructured light illumination and elucidated the role of the OAM in the scattering response of the all-dielectric meta-atoms with arbitrary shapes and orientations, enabling new ways of manipulating their optical responses on demand and/or in time-modulated fashion.[100–105]

5. Conclusion

In summary, we investigated the synergy between structured light and meta-atoms as a new degree of freedom for engineering the spectral response of the all-dielectric nanostructures. In particular, we performed a detailed study of an LG light beam impinging on an individual polycrystalline silicon-based nanocuboid and nanocylinder and compared its corresponding results with the case of Gaussian beam illumination. We predicted and demonstrated the emergence of additional resonant peaks upon the introduction of phase discontinuity to the incoming beam that can be tuned by changing the topological charge and the angle of incidence of the incoming beam. By exploiting the semi-analytical multipole decomposition approach, we showed that these newly emerged peaks in the scattering response are attributed to one of the families of higher-order multipolar moments excited within the structure. Moreover, we studied the role of the topological charge in the optical response of a cylindrical meta-atom and showed how its corresponding scattering response varies from a dip to a peak once the topological charge of the incoming beam changes from $m = 0$ to $m = 1$. Furthermore, it was revealed that the phase asymmetry-induced higher-order multipole resonances can be affected by the meta-atom rotation, or equivalently illumination direction. The presented concept of OAM-based manipulation of Mie-type resonances of arbitrary-shaped meta-atoms has several potential applications ranging from remote sensing relying on the shape and orientation of meta-atoms, to spectroscopy, and light transmission in scattering media.

Supporting Information

Supporting Information is available from the Wiley Online Library or from the author.

Acknowledgements

This paper was supported in part by the Office of Naval Research (ONR) (Grant No. N00014-20-1-2558), National Science Foundation (NSF) (Grant No. 1809518), and Army Research Office Award (Grant No. W911NF1810348). The polysilicon refractive index was obtained from the ellipsometry measurement on the samples that were provided at the Center for Nanophase Materials Sciences, which is a DOE Office of Science User Facility.

Conflict of Interest

The authors declare no conflict of interest.

Data Availability Statement

The data that support the findings of this study are available from the corresponding author upon reasonable request.

Keywords

high-index nanoparticles, Mie resonances, multipole decomposition, structured light

Received: June 25, 2022
Revised: November 25, 2022
Published online: January 6, 2023

[1] Y. Kivshar, A. Miroshnichenko, *Opt. Photonics News* **2017**, *28*, 24.
[2] M. I. Mishchenko, *J. Quant. Spectrosc. Radiat. Transfer* **2009**, *110*, 1210.
[3] Y. Kivshar, *Nano Lett.* **2022**, *22*, 3513.
[4] N. Meinzer, W. L. Barnes, I. R. Hooper, *Nat. Photonics* **2014**, *8*, 889.
[5] T. Liu, R. Xu, P. Yu, Z. Wang, J. Takahara, *Nanophotonics* **2020**, *9*, 1115.
[6] A. I. Kuznetsov, A. E. Miroshnichenko, M. L. Brongersma, Y. S. Kivshar, B. Luk'yanchuk, *Science* **2016**, *354*, 2472.
[7] Y. Kivshar, *Natl. Sci. Rev.* **2018**, *5*, 144.
[8] I. Staude, J. Schilling, *Nat. Photonics* **2017**, *11*, 274.
[9] S. Kruk, Y. Kivshar, *ACS Photonics* **2017**, *4*, 2638.
[10] W. Liu, Y. S. Kivshar, *Opt. Express* **2018**, *26*, 13085.
[11] A. I. Kuznetsov, A. E. Miroshnichenko, Y. H. Fu, J. Zhang, B. Luk'yanchuk, *Sci. Rep.* **2012**, *2*, 492.
[12] Y. H. Fu, A. I. Kuznetsov, A. E. Miroshnichenko, Y. F. Yu, B. Luk'yanchuk, *Nat. Commun.* **2013**, *4*, 1527.
[13] U. Zywietz, A. B. Evlyukhin, C. Reinhardt, B. N. Chichkov, *Nat. Commun.* **2014**, *5*, 3402.

[14] M. L. Brongersma, Y. Cui, S. Fan, *Nat. Mater.* **2014**, *13*, 451.
[15] R. Verre, D. G. Baranov, B. Munkhbat, J. Cuadra, M. Käll, T. Shegai, *Nat. Nanotechnol.* **2019**, *14*, 679.
[16] R. Mupparapu, T. Bucher, I. Staude, *Adv. Phys.: X* **2020**, *5*, 1734083.
[17] Z.-X. Zhou, M.-J. Ye, M.-W. Yu, J.-H. Yang, K.-L. Su, C.-C. Yang, C.-Y. Lin, V. E. Babicheva, I. V. Timofeev, K.-P. Chen, *ACS Nano* **2022**, *16*, 5994.
[18] G. Grinblat, Y. Li, M. P. Nielsen, R. F. Oulton, S. A. Maier, *ACS Photonics* **2017**, *4*, 2144.
[19] D. E. Utkin, K. V. Anikin, S. L. Veber, A. A. Shklyaev, *Opt. Mater.* **2020**, *109*, 110466.
[20] J. Jang, T. Badloe, Y. C. Sim, Y. Yang, J. Mun, T. Lee, Y.-H. Cho, J. Rho, *Nanoscale* **2020**, *12*, 21392.
[21] H. Wang, J. Wang, S. Li, K. H. Li, H.-Q. Lin, L. Shao, Anapole-Mediated Emission Enhancement in Gallium Nitride Nanocavities. *arXiv preprint arXiv:2111.08937* **2021**.
[22] N. K. Emani, E. Khaidarov, R. Paniagua-Domínguez, Y. H. Fu, V. Valuckas, S. Lu, X. Zhang, S. T. Tan, H. V. Demir, A. I. Kuznetsov, *Appl. Phys. Lett.* **2017**, *111*, 221101.
[23] Z. Sun, B. Xu, B. Wu, X. Wang, H. Ying, *Nanomaterials* **2021**, *11*, 2638.
[24] K. Koshelev, Y. Kivshar, *ACS Photonics* **2020**, *8*, 102.
[25] D. G. Baranov, D. A. Zuev, S. I. Lepeshov, O. V. Kotov, A. E. Krasnok, A. B. Evlyukhin, B. N. Chichkov, *Optica* **2017**, *4*, 814.
[26] P. D. Terekhov, H. K. Shamkhi, E. A. Gurvitz, K. V. Baryshnikova, A. B. Evlyukhin, A. S. Shalin, A. Karabchevsky, *Opt. Express* **2019**, *27*, 10924.
[27] M. Wu, S. T. Ha, S. Shendre, E. G. Durmusoglu, W.-K. Koh, D. R. Abujetas, J. A. Sánchez-Gil, R. Paniagua-Domínguez, H. V. Demir, A. I. Kuznetsov, *Nano Lett.* **2020**, *20*, 6005.
[28] W. Zhu, R. Yang, G. Geng, Y. Fan, X. Guo, P. Li, Q. Fu, F. Zhang, C. Gu, J. Li, *Nanophotonics* **2020**, *9*, 4327.
[29] M. Semmlinger, M. Zhang, M. L. Tseng, T.-T. Huang, J. Yang, D. P. Tsai, P. Nordlander, N. J. Halas, *Nano Lett.* **2019**, *19*, 8972.
[30] V. R. Tuz, A. B. Evlyukhin, *Nanophotonics* **2021**, *10*, 4373.
[31] S. Lepeshov, Y. Kivshar, *ACS Photonics* **2018**, *5*, 2888.
[32] G. Zhang, C. Lan, R. Gao, Y. Wen, J. Zhou, *Adv. Theory Simul.* **2019**, *2*, 1900123.
[33] M. I. Shalaev, J. Sun, A. Tsukernik, A. Pandey, K. Nikolskiy, N. M. Litchinitser, *Nano Lett.* **2015**, *15*, 6261.
[34] P. C. Wu, R. A. Pala, G. K. Shirmanesh, W.-H. Cheng, R. Sokhoyan, M. Grajower, M. Z. Alam, D. Lee, H. A. Atwater, *Nat. Commun.* **2019**, *10*, 3654.
[35] W. Liu, A. E. Miroshnichenko, *ACS Photonics* **2017**, *5*, 1733.
[36] T. Cui, B. Bai, H.-B. Sun, *Adv. Funct. Mater.* **2019**, *29*, 1806692.
[37] L. Kang, R. P. Jenkins, D. H. Werner, *Adv. Opt. Mater.* **2019**, *7*, 1801813.
[38] X. Zhao, J. Schalch, J. Zhang, H. R. Seren, G. Duan, R. D. Averitt, X. Zhang, *Optica* **2018**, *5*, 303.
[39] G. Zheng, H. Mühlenbernd, M. Kenney, G. Li, T. Zentgraf, S. Zhang, *Nat. Nanotechnol.* **2015**, *10*, 308.
[40] L. Huang, S. Zhang, T. Zentgraf, *Nanophotonics* **2018**, *7*, 1169.
[41] X. Ni, A. V. Kildishev, V. M. Shalaev, *Nat. Commun.* **2013**, *4*, 2807.
[42] J. Gao, M. A. Vincenti, J. Frantz, A. Clabeau, X. Qiao, L. Feng, M. Scalora, N. M. Litchinitser, *Nanophotonics* **2022**, *11*, 4027.
[43] J. Gao, M. A. Vincenti, J. Frantz, A. Clabeau, X. Qiao, L. Feng, M. Scalora, N. M. Litchinitser, *Nat. Commun.* **2021**, *12*, 5833.
[44] A. Krasnok, M. Tymchenko, A. Alù, *Mater. Today* **2018**, *21*, 8.
[45] A. E. Minovich, A. E. Miroshnichenko, A. Y. Bykov, T. V. Murzina, D. N. Neshev, Y. S. Kivshar, *Laser Photonics Rev.* **2015**, *9*, 195.
[46] H. K. Shamkhi, K. V. Baryshnikova, A. Sayanskiy, P. Kapitanova, P. D. Terekhov, P. Belov, A. Karabchevsky, A. B. Evlyukhin, Y. Kivshar, A. S. Shalin, *Phys. Rev. Lett.* **2019**, *122*, 193905.
[47] H. K. Shamkhi, A. Sayanskiy, A. C. Valero, A. S. Kupriianov, P. Kapitanova, Y. S. Kivshar, A. S. Shalin, V. R. Tuz, *Phys. Rev. Mater.* **2019**, *3*, 085201.
[48] X. Zhang, A. L. Bradley, *Phys. Rev. B* **2021**, *103*, 195419.
[49] J. A. Schuller, R. Zia, T. Taubner, M. L. Brongersma, *Phys. Rev. Lett.* **2007**, *99*, 107401.
[50] A. B. Evlyukhin, C. Reinhardt, A. Seidel, B. S. Luk'yanchuk, B. N. Chichkov, *Phys. Rev. B* **2010**, *82*, 045404.
[51] A. García-Etxarri, R. Gómez-Medina, L. S. Froufe-Pérez, C. López, L. Chantada, F. Scheffold, J. Aizpurua, M. Nieto-Vesperinas, J. J. Sáenz, *Opt. Express* **2011**, *19*, 4815.
[52] A. B. Evlyukhin, C. Reinhardt, B. N. Chichkov, *Phys. Rev. B* **2011**, *84*, 235429.
[53] A. B. Evlyukhin, S. M. Novikov, U. Zywietz, R. L. Eriksen, C. Reinhardt, S. I. Bozhevolnyi, B. N. Chichkov, *Nano Lett.* **2012**, *12*, 3749.
[54] S. Person, M. Jain, Z. Lapin, J. J. Sáenz, G. Wicks, L. Novotny, *Nano Lett.* **2013**, *13*, 1806.
[55] G. Gouesbet, B. Maheu, G. Gréhan, *J. Opt. Soc. Am. A* **1988**, *5*, 1427.
[56] C. Rotschild, S. Zommer, S. Moed, O. Hershcovitz, S. G. Lipson, *Appl. Opt.* **2004**, *43*, 2397.
[57] V. V. Kotlyar, H. Elfstrom, J. Turunen, A. A. Almazov, S. N. Khonina, V. A. Soifer, *J. Opt. Soc. Am. A* **2005**, *22*, 849.
[58] A. Rubano, F. Cardano, B. Piccirillo, L. Marrucci, *J. Opt. Soc. Am. B* **2019**, *36*, D70.
[59] W. Ji, C.-H. Lee, P. Chen, W. Hu, Y. Ming, L. Zhang, T.-H. Lin, V. Chigrinov, Y.-Q. Lu, *Sci. Rep.* **2016**, *6*, 25528.
[60] L. Marrucci, *J. Nanophotonics* **2013**, *7*, 078598.
[61] C. Rosales-Guzmán, A. Forbes. *How to Shape Light with Spatial Light Modulators*, SPIE Press, Bellingham, WA **2017**.
[62] F. Yue, D. Wen, J. Xin, B. D. Gerardot, J. Li, X. Chen, *ACS Photonics* **2016**, *3*, 1558.
[63] H. Barati Sedeh, M. M. Salary, H. Mosallaei, *Nanophotonics* **2020**, *9*, 2957.
[64] A. Forbes, M. De Oliveira, M. R. Dennis, *Nat. Photonics* **2021**, *15*, 253.
[65] H. Rubinsztein-Dunlop, A. Forbes, M. V. Berry, M. R. Dennis, D. L. Andrews, M. Mansuripur, C. Denz, C. Alpmann, P. Banzer, T. Bauer, E. Karimi, L. Marrucci, M. Padgett, M. Ritsch-Marte, N. M. Litchinitser, N. P. Bigelow, C. Rosales-Guzmán, A. Belmonte, J. P. Torres, T. W. Neely, M. Baker, R. Gordon, A. B. Stilgoe, J. Romero, A. G. White, R. Fickler, A. E. Willner, G. Xie, B. Mcmorran, A. M. Weiner, *J. Opt.* **2016**, *19*, 013001.
[66] D. L. Andrews, *Structured Light and Its Applications: An Introduction to Phase-Structured Beams and Nanoscale Optical Forces*, Academic Press, Burlington, MA **2011**.
[67] P. Woźniak, P. Banzer, G. Leuchs, *Laser Photonics Rev.* **2015**, *9*, 231.
[68] T. Das, P. P. Iyer, R. A. Decrescent, J. A. Schuller, *Phys. Rev. B* **2015**, *92*, 241110.
[69] J. Zeng, M. Darvishzadeh-Varcheie, M. Albooyeh, M. Rajaei, M. Kamandi, M. Veysi, E. O. Potma, F. Capolino, H. K. Wickramasinghe, *ACS Nano* **2018**, *12*, 12159.
[70] Z. Xi, L. Wei, A. J. L. Adam, H. P. Urbach, *Opt. Lett.* **2016**, *41*, 33.
[71] L. Wei, N. Bhattacharya, H. Paul Urbach, *Opt. Lett.* **2017**, *42*, 1776.
[72] A. E. Miroshnichenko, A. B. Evlyukhin, Y. F. Yu, R. M. Bakker, A. Chipouline, A. I. Kuznetsov, B. Luk'yanchuk, B. N. Chichkov, Y. S. Kivshar, *Nat. Commun.* **2015**, *6*, 8069.
[73] K. V. Baryshnikova, D. A. Smirnova, B. S. Luk'yanchuk, Y. S. Kivshar, *Adv. Opt. Mater.* **2019**, *7*, 1801350.
[74] Y. Yang, S. I. Bozhevolnyi, *Nanotechnology* **2019**, *30*, 204001.
[75] R. Masoudian Saadabad, L. Huang, A. B. Evlyukhin, A. E. Miroshnichenko, *Opt. Mater. Express* **2022**, *12*, 1817.
[76] T. Raybould, V. A. Fedotov, N. Papasimakis, I. Youngs, N. I. Zheludev, *Appl. Phys. Lett.* **2017**, *111*, 081104.
[77] L. Wei, Z. Xi, N. Bhattacharya, H. P. Urbach, *Optica* **2016**, *3*, 799.

[78] A. G. Lamprianidis, A. E. Miroshnichenko, *Beilstein J. Nanotechnol.* **2018**, *9*, 1478.
[79] R. Masoudian Saadabad, M. Cai, F. Deng, L. Xu, A. E. Miroshnichenko, *Phys. Rev. B* **2021**, *104*, 165402.
[80] E. V. Melik-Gaykazyan, K. L. Koshelev, J.-H. Choi, S. S. Kruk, H.-G. Park, A. A. Fedyanin, Y. S. Kivshar, *JETP Lett.* **2019**, *109*, 131.
[81] E. V. Melik-Gaykazyan, S. S. Kruk, R. Camacho-Morales, L. Xu, M. Rahmani, K. Zangeneh Kamali, A. Lamprianidis, A. E. Miroshnichenko, A. A. Fedyanin, D. N. Neshev, Y. S. Kivshar, *ACS Photonics* **2017**, *5*, 728.
[82] X. Zambrana-Puyalto, X. Vidal, G. Molina-Terriza, *Opt. Express* **2012**, *20*, 24536.
[83] C. Sanz-Fernández, M. Molezuelas-Ferreras, J. Lasa-Alonso, N. de Sousa, X. Zambrana-Puyalto, J. Olmos-Trigo, *Laser Photonics Rev.* **2021**, *15*, 2100035.
[84] A. B. Evlyukhin, T. Fischer, C. Reinhardt, B. N. Chichkov, *Phys. Rev. B* **2016**, *94*, 205434.
[85] A. B. Evlyukhin, B. N. Chichkov, *Phys. Rev. B* **2019**, *100*, 125415.
[86] A. B. Evlyukhin, C. Reinhardt, E. Evlyukhin, B. N. Chichkov, *J. Opt. Soc. Am. B* **2013**, *30*, 2589.
[87] P. Grahn, A. Shevchenko, M. Kaivola, *New J. Phys.* **2012**, *14*, 093033.
[88] V. M. Dubovik, V. V. Tugushev, *Phys. Rep.* **1990**, *187*, 145.
[89] J. Chen, J. Ng, Z. Lin, C. T. Chan, *Nat. Photonics* **2011**, *5*, 531.
[90] P. Woźniak, I. De Leon, K. Höflich, G. Leuchs, P. Banzer, *Optica* **2019**, *6*, 961.
[91] P. Woźniak, I. De Leon, K. Höflich, C. Haverkamp, S. Christiansen, G. Leuchs, P. Banzer, *Opt. Express* **2018**, *26*, 19275.
[92] A. E. Krasnok, A. E. Miroshnichenko, P. A. Belov, Y. S. Kivshar, *Opt. Express* **2012**, *20*, 20599.
[93] D. Arslan, K. E. Chong, A. E. Miroshnichenko, D.-Y. Choi, D. N. Neshev, T. Pertsch, Y. S. Kivshar, I. Staude, *J. Phys. D: Appl. Phys.* **2017**, *50*, 434002.
[94] J. Sancho-Parramon, S. Bosch, *ACS Nano* **2012**, *6*, 8415.
[95] P. Banzer, U. Peschel, S. Quabis, G. Leuchs, *Opt. Express* **2010**, *18*, 10905.
[96] T. Züchner, A. V. Failla, A. Hartschuh, A. J. Meixner, *J. Microsc.* **2008**, *229*, 337.
[97] T. Bauer, S. Orlov, G. Leuchs, P. Banzer, *Appl. Phys. Lett.* **2015**, *106*, 091108.
[98] X. Zambrana-Puyalto, X. Vidal, P. Woźniak, P. Banzer, G. Molina-Terriza, *ACS Photonics* **2018**, *5*, 2936.
[99] P. Woźniak, I. De Leon, K. Höflich, G. Leuchs, P. Banzer, *Optica* **2019**, *6*, 961.
[100] G. Ptitcyn, M. S. Mirmoosa, S. A. Tretyakov, *Phys. Rev. Res.* **2019**, *1*, 023014.
[101] M. S. Mirmoosa, T. T. Koutserimpas, G. A. Ptitcyn, S. A. Tretyakov, R. Fleury, *New J. Phys.* **2022**, *24*, 063004.
[102] H. Barati Sedeh, M. M. Salary, H. Mosallaei, *Nanophotonics* **2020**, *9*, 2957.
[103] H. Barati Sedeh, M. M. Salary, H. Mosallaei, *Adv. Opt. Mater.* **2020**, *8*, 2000075.
[104] H. Barati Sedeh, M. M. Salary, H. Mosallaei, *Laser Photonics Rev.* **2022**, *16*, 2100449.
[105] V. Pacheco-Peña, N. Engheta, *New J. Phys.* **2021**, *23*, 095006.